Excitonic emissions and above-band-gap luminescence in the single-crystal perovskite semiconductors CsPbBr_{3} and CsPbCl_{3}

M. Sebastian, J. A. Peters, C. C. Stoumpos, J. Im, S. S. Kostina, Z. Liu, M. G. Kanatzidis, A. J. Freeman, and B. W. Wessels

Phys. Rev. B **92**, 235210 — Published 29 December 2015

DOI: 10.1103/PhysRevB.92.235210

Excitonic Emissions and Above-Bandgap Luminescence in Single Crystal Perovskite Semiconductors $CsPbBr_3$ and $CsPbCl_3$

M. Sebastian[1], J.A. Peters[1], C. C. Stoumpos[2], J. Im[3], S. S. Kostina[1], Z. Liu[1], M.G. Kanatzidis[2], A. J. Freeman[3], and B. W. Wessels[1]

1 Dept. of Materials Science, Northwestern University, Evanston, IL 60208

2 Dept. of Chemistry, Northwestern University, Evanston, IL 60208

3 Dept. of Physics and Astronomy, Northwestern University, Evanston, IL 60208

Abstract

The ternary compounds $CsPbX_3$ (X= Br or Cl) have perovskite structures that are being considered for optical and electronic applications such as lasing and gamma ray detection. Above bandgap excitonic photoluminescence (PL) band is seen in both $CsPbX_3$ compounds. An excitonic emission peak centered at 2.98 eV, ~0.1 eV above the room temperature bandgap, is observed for $CsPbCl_3$. The thermal quenching of the excitonic luminescence is well described by a two-step quenching model, yielding activation energies of 0.057 eV and 0.0076 eV for high and low temperature regimes, respectively. $CsPbBr_3$ exhibits bound excitonic luminescence peaks located at 2.29 eV and 2.33 eV that are attributed to recombination involving Br vacancy centers. Activation energies for thermal quenching of the excitonic luminescence of 0.017 eV and 0.0007 eV were calculated for $CsPbBr_3$. Temperature dependent PL experiments reveal unexpected blueshifts for all excitonic emission peaks in $CsPbX_3$ compounds. A phonon assisted step-up process leads to the blueshift in $CsPbBr_3$ emission, while there is a contribution from bandgap widening in $CsPbCl_3$. The absence of significant deep level defect luminescence in these compounds makes them attractive candidates for high resolution, room temperature radiation detection.

Keywords: photoluminescence (PL), exciton emission, gamma-ray detection, perovskite halides, $CsPbBr_3$, $CsPbCl_3$

I. Introduction

The last few years have witnessed a dramatic increase of research on the halide perovskite compounds of group IV metal ions. This long-known class of semiconductors has been studied starting as far back as 1950's, mainly through the pioneering work of Moller on the $CsPbX_3$ compound (X = Cl, Br, I)[1,2]. Since then, these perovskite compounds have attracted much attention due to their remarkable optical[3,4,5,6] and electronic[7] properties and the numerous temperature-induced structural phase transitions[8]. The discovery that ignited the recent explosive growth in the field was the realization of efficient Dye-Sensitized Solar Cells (DSSC's) using perovskite structure $CH_3NH_3PbI_3$ as the light-absorbing component, thus achieving a 4% conversion efficiency[9]. After the initial discovery, the liquid electrolyte was eliminated in favor of an all-solid state photovoltaic device, marked by the successful employment of $CsSnI_3$[10] and $CH_3NH_3PbI_3$-based perovskites[11] as hole transport and light-absorber components, respectively. Currently, the perovskite solar cells are able to deliver conversion efficiencies of ~20%[12], clearly demonstrating the excellent photoconducting properties of the halide perovskite semiconductors. However, aside from the initial reports on photoconductivity of the $CsPbX_3$ compounds [1] only few experiments dealt with the charge-transport properties of these compounds and in most of them the measured electrical properties were attributed to ionic motion[13]. We recently focused our attention in the development of $CsPbX_3$[14,15] and other halide semiconductor compounds[16] to utilize their photo-conversion potential in the field of high energy radiation detection.

Gamma ray spectroscopy is widely used in fields such as security, medicine, and astrophysics. For many of these applications, it is important to have materials that are able to detect gamma rays with high energy resolution at room temperature. This can be achieved by using semiconductors that have a large bandgap, high density, and optimal charge transport properties as given by the mobility-lifetime (μτ) product. Current detector materials are semi-insulating semiconductors containing heavy elements, such as $Cd_{0.9}Zn_{0.1}Te$ (CZT) and TlBr [17]. These semiconductors have high resistivities (>10^9 Ω-cm) that result in low detector background noise, leading to high resolution gamma ray spectra. In addition the semiconductor CZT has a μτ value on the order of 10^{-2} $cm^2 \cdot V^{-1}$ and TlBr on the order of 10^{-3} $cm^2 \cdot V^{-1}$. There are, however, several drawbacks associated with these two compounds. CZT is known to exhibit twinning and Te precipitation formation that lowers the μτ value, whereas TlBr is mechanically soft and thus deleterious line defects are readily formed. In addition, TlBr suffers from electric polarization over time [17,18], which results in a built-in field that impedes current flow in the material, causing a decrease in detector performance over time. These effects limit the detector efficiency and its spectral resolution.

As a result, other compounds such as the ternary compounds $CsPbX_3$ (X = Br, Cl) are being considered as room temperature x-ray and gamma ray detector materials due to their high density, high resistivity, μτ and wide bandgap [14,15]. Large single crystals of these compounds were grown via modified Bridgman technique. They have direct bandgaps and high μτ values on the order of 10^{-3} $cm^{2}\cdot V^{-1}$ for both electrons and holes stemming from the favorable electronic structure of the perovskite structure-type. In addition, $CsPbBr_3$ has already been shown to detect Ag X-rays [14,15]. Since these compounds are being considered as hard radiation detector materials, a number of relevant properties such as defect stability need to be understood. Even very low concentrations of native defects and impurities can serve as traps and recombination centers that degrade the detector performance [17]. Trapping of photo-excited carriers at defects decreases spectral resolution. Furthermore, surface recombination of carriers decreases the charge collection efficiency. The μτ value of a material is degraded by defect concentrations as low as a few ppm or even lower. Most chemically specific measurement techniques do not have the requisite sensitivity to detect defects at these low levels. In addition, they cannot detect native defects such as vacancies and anti-site defects which can also result in decreased μτ values and detector efficiency. However, since many of these point defects are luminescent they can be detected by photoluminescence (PL) spectroscopy. Substitutional chemical impurities and native defects such as vacancies can manifest themselves as peaks in a PL spectrum, even at concentrations in the parts per billion range.

There are several prior PL studies of single crystal $CsPbX_3$ compounds [3,5,14,15,19-21]. PL measurements on single crystal samples of $CsPbBr_3$ have shown the presence of emission bands at 2.32 eV at temperatures up to 110 K that have been attributed to recombination of free excitons [3,5,14,15,19]. At 4.2 K, this peak is accompanied by several phonon replicas [3,19]. If this emission is indeed due to the free exciton it suggests that the compounds are nominally chemically pure and stoichiometric. However, a subsequent study of PL of single crystals of $CsPbBr_3$ grown by Bridgman revealed the presence of a broad peak below the band edge at 2.16 eV from 6 K up to 90 K [5]. This was attributed to emission from a defect or series of defect states, whose nature was not further investigated [5]. Previous PL measurements on single crystal $CsPbCl_3$ indicated the presence of a free exciton peak at 2.98 eV, with additional peaks reported at 2.97, 2.96, and 2.94 eV [3]. The peak at 2.97 eV was tentatively attributed to either a bound exciton or band edge luminescence, the peak at 2.96 eV to a phonon replica of the free exciton peak, and the peak at 2.94 eV was defect-related, possibly a bound exciton.

Here we report on temperature and power dependent PL measurements of undoped $CsPbX_3$ Bridgman grown single crystals. Thermal quenching measurements enable determination of the activation energies of the luminescent defects [22,23]. Power dependent PL measurements are used to determine the defect species involved in radiative recombination: excitonic, donor-acceptor pair (DAP), or free-to-bound excitonic transitions [22,24]. For $CsPbBr_3$, luminescence emission is observed at 2.33 eV and 2.29 eV at 10 K, persisting up to room temperature. For $CsPbCl_3$, an excitonic peak is observed at 2.98 eV, along with additional peaks at 2.94, 2.96, and 2.97eV. In both compounds the luminescence emission is above the conduction band edge and is tentatively attributed to recombination involving halogen vacancy defect centers. Neither shallow nor deep level radiative defects are observed within the gap in these $CsPbX_3$ compounds.

II. Experiment

Single crystal ingots of the compounds were grown by the vertical Bridgman method using a four zone furnace with the temperature in the two top zones set to 700^0C and the two lower zones operating at 300^0C. The $CsPbBr_3$ samples reported in this study were synthesized as follows: $PbBr_2$ is dissolved in 48% aqueous HBr and added slowly, under constant stirring at the initial steps, to a solution of CsBr dissolved in water. The mixture is left to cool down to ambient temperature and immediately filtered through a fritted-dish funnel under vacuum. The solid is washed with 8% aqueous HBr followed by methanol and dried overnight. The solid is further dried in an oven at ~ 70^0C in air. $CsPbCl_3$ was prepared similarly, with Cs_2CO_3 dissolved in 37% aqueous HCl being slowly added to PbO dissolved in 37% aqueous HCl under constant stirring to form the compound. The resulting $CsPbCl_3$ is filtered and dried as described above and then washed with 6% aqueous HCl followed by methanol and left for overnight drying. The solid is further dried in an oven at ~ 70^0C in air. Further details of $CsPbX_3$ synthesis, growth, and processing are presented elsewhere [15]. Small crystals that were suitable for X-ray diffraction were readily obtained from the boule and mounted on a STOE II image plate single-crystal diffractometer. Powder X-ray diffraction measurements were performed using a siliconcalibrated CPS 120 INEL powder X-ray diffractometer (Cu Kα, 1.54056A°) graphite monochromatized radiation) operating at 40 kV and 20 mA. The crystal structures of the compounds were solved and refined using the SHELXL-2013 suite[25], aided by special functions of the PLATON[26] and WINGX[27] program suites. The as-grown crystal is semi-insulating with a resistivity ~10^{10} Ω-cm [15].

For PL measurements, the 405 nm line from a CW semiconductor diode laser is the excitation source. For temperature-dependent PL measurements, the excitation intensity was kept constant at 31.6 mW for $CsPbBr_3$ and at 15.8 mW for $CsPbCl_3$ as this was found to give the maximum overall PL intensity at 10K. For the power-dependent PL measurement, the same excitation source was used, with a series of neutral optical density filters employed to vary the incident laser power from 2.0 to up to 50 mW for $CsPbCl_3$ and from 2.0 to up to 91 mW for $CsPbBr_3$. An optical chopper and lock-in amplifier were used to improve signal to noise ratio. The PL emission spectra were resolved through the 0.75 m SPEX grating monochromator and detected by a Hamamatsu photomultiplier tube (R928). The sample was cooled to 10 K using a closed-cycle He cryostat (SHI cryogenics DE-202).

First-principles calculations were performed in order to determine thermodynamic properties of intrinsic defects for the case of $CsPbBr_3$. The projector augmented wave method[28] was implemented in the VASP code [29]. The generalized gradient approximation (GGA) method within the Perdew-Burke-Ernzerhof formalism [30] was employed for the exchange correlation functional, and the Heyd-Scuseria-Ernzerhof hybrid functional[31] was used to correct the band gap underestimation of the semi-local functional. The formation energy of defect D in charge state $q(\Delta H_{D,q})$was calculated with the following formula,

$$\Delta H_{D,q} = E(D^q) - E(Bulk) - \sum_i n_i\mu_i + qE_F + E_{corr}, \quad 1$$

where E is the total energy of a bulk or a defect system in a charge state q, n_i is a number of the atom i which is removed (n<0) or added (n>0) to form defect D, μ_i is the corresponding chemical potential of the element i, and E_F is the Fermi level [32]. Chemical potential μ_i is determined with a growth condition and Fermi level E_F is determined self-consistently within the charge neutrality condition under the given growth temperature (T_g). E_{corr} is a correction term including the finite cell correction [33] and band gap correction [34]. The defect level was determined with the charge transition level from q to q' $\varepsilon(q/q')$defined by

$$\varepsilon(q/q') = \left(\Delta H_D(D,q) - \Delta H_D(D,q')\right)/(q'-q) \quad 2$$

To describe isolated defect configurations, a 2x2x2 supercell which accommodates 160 atoms was used. A 3x3x3 k-point mesh was used for momentum space integration.

III. Results and discussion

Temperature-dependent PL studies

The PL spectra of $CsPbBr_3$ from 10 K to 180 K are shown in Fig. 1a. Scans from 1.5 to 3.0 eV show a single narrow emission peak centered at ~2.32 eV. The inset of Fig. 1a shows the decomposition of the spectrum at 10 K, where 2 peaks (at 2.33 eV and 2.29 eV) are observed using a Gaussian decomposition. The luminescence spectrum of $CsPbBr_3$ over a wide sub-band-gap energy range and increased sensitivity is shown in Fig. 1c. The semi-log plot indicates that no significant concentration of deep level defects exist in the compound. The peak centered at 2.33 eV has been previously assigned to a free exciton peak emission [3,5,19], while the peak located at 2.29 eV has been previously attributed to either a phonon replica of the free exciton [3] or to recombination involving a bound exciton state[5]. Absorption spectra obtained from a polished single crystal of $CsPbBr_3$ using UV-Vis-IR transmission measurements as well as from a powdered $CsPbBr_3$ sample using diffuse reflectance (Fig. 2a) indicate that the room temperature bandgap for $CsPbBr_3$ crystal is ~2.23 eV. This value is in agreement with that previously reported [14,15]. As can be seen from Fig. 2a, the absorption edge does not match the energy of the room temperature PL emission. Thus it is concluded that the observed excitonic emission in these compounds is not due to band-to-band recombination as previously reported. This suggests that the luminescence involves a level above the conduction band edge. We also note that the powder absorption spectra of both $CsPbX_3$ samples (Fig. 2c) reveal a feature above the band edge that roughly aligns with the emission peak position. However, the origin of this absorption feature is currently unknown.

The origin of the above bandgap luminescence in $CsPbBr_3$ was investigated using DFT calculations to determine the electronic states of defects. States ~0.23 eV and ~0.24 eV above the conduction band edge due to Br vacancies are predicted. These calculations indicate that a recombination via bound excitons exists that should result in PL peaks with energies of ~2.46 eV and ~2.47 eV, respectively. These calculations of defect levels are in reasonable agreement with earlier DFT calculations on this compound by Shi and Du[35] which indicated a Br vacancy located at 0.16 eV above the conduction band minimum. The observed room temperature PL peak located at ~2.38 eV (~0.16 eV above the bandgap) is thus tentatively attributed to recombination via a bound exciton involving a Br vacancy defect. In the observed luminescence, electrons are trapped by the Br vacancy defect and form a bound exciton with free holes in the valence band. Recently, such above bandgap PL emission at room temperature in organo-lead halide perovskite $CH_3NH_3PbI_3$ was observed but in that case it was attributed to free carrier generation through rapid exciton dissociation [36]. While not typical, above-bandgap PL has also been observed in dilute $GaAs_{1-x}N_x$ alloys[37] and $GaAs_{1-x}P_x$[38]. For the case of $GaAs_{1-x}P_x$, the above-bandgap emission was ascribed to recombination involving isoelectronic N traps with levels above the conduction band edge. In the case of $GaAs_{1-x}N_x$ alloys, the above-bandgap emission however was attributed to a collection of perturbed conduction band states near the *L* point. In the present case, a physical model of the PL process for the 2.38 eV peak can be described as follows: incident photons are absorbed by promoting electrons from the valence band into higher excited states in the conduction band. Upon relaxation, an electron is then captured/trapped at a localized Br vacancy defect with energy level degenerate with conduction band states. This is followed by the captured electron combining with a free hole in the valence band to form a bound exciton.

PL studies of $CsPbCl_3$ in the 1.5 to 3.0 eV range reveal a narrow peak overlapped on a broad shoulder centered at ~2.97 eV (Fig. 1b). The luminescence spectrum in a wide sub-band-gap energy range and increased sensitivity is shown on a semi-log plot in Fig. 1c. It is possible that an extremely weak broad sub-gap emission (~2.3 - 2.6 eV) is present in $CsPbCl_3$. However, it is 10^4 times weaker than the dominant peak and thus only an extremely low concentration of deep level defects exist in $CsPbCl_3$. Gaussian decomposition of the PL signals below 100 K reveals four peaks centered at 2.94, 2.96, 2.97, and 2.98 eV (Fig. 1b inset). Above 100K and up to 290 K, only the latter three peaks listed are observed. This is to be compared to the room temperature bandgap for $CsPbCl_3$ crystals which is 2.85 eV (Fig. 2b). Thus all the PL emission peaks in Fig. 2b are above the bandgap. The peak centered at 2.98 eV could presumably be attributed to an exciton bound to a higher-lying defect state within the conduction band such as in the case for $CsPbBr_3$; with phonon replicas centered at 2.96 eV and 2.94 eV. A peak at 2.97 eV in $CsPbCl_3$ was previously attributed to a bound exciton [3], which is likely the identity of the 2.97 eV peak in this study.

Another possible interpretation of the observed emission band at 2.98 eV is luminescence from a larger bandgap nanocrystalline inclusions embedded in the monocrystalline matrix. Luminescence of $CsPbCl_3$ nanocrystals embedded in CsCl:Pb single crystals has been previously reported [39], where an above bandgap peak at 2.98 eV was observed at 10 K. Similarly, $CsPbBr_3$-like quantum dots exhibit PL emission in the 2.34-2.48 eV range at 5 K, which is above the bandgap energy of $CsPbBr_3$ single crystals and more closely matches that of $CsPbBr_3$ thin films [6]. However, pXRD results in the present study, shown in Fig. 2c, indicate that the crystals are phase-pure and therefore it is unlikely that we have nanoprecipitates in our $CsPbX_3$ samples. Alternatively, the observed recombination in $CsPbX_3$ could be associated with a higher lying conduction band edge. Furthermore, DFT calculations in the present study indicate that there are several higher lying conduction bands within 0.2 – 0.5 eV of the lowest lying conduction band edge.

All emission peaks of $CsPbBr_3$ and $CsPbCl_3$ blueshift with increasing temperature (Figs. 3a and 3b, respectively). This is unexpected since excitonic PL typically redshifts with increasing temperature due to bandgap shrinkage [40]. Although there have been reports of blueshifting of the absorption edge with increasing temperature in other Pb-based semiconductors [41], this behavior has not been reported for $CsPbBr_3$. However, in the case of CdMnTe crystals blueshifting of a Mn^{2+} emission peak with temperature above 60 K has been observed. The ~ 0.04 eV shift was attributed to a multiphonon-assisted step-up process [42]. In this process, the carriers can reach a higher energy state due to phonon absorption, which is enhanced with increasing temperature. The observed blueshift of emission peaks with temperature in $CsPbBr_3$ by ~0.04 eV (Fig. 3a) is consistent with such a multiphonon process.

In the case of $CsPbCl_3$ the blueshift of the emission peaks is also unexpected (Fig. 3b).

The blueshift of the excitonic luminescence spectra has been previously observed in the 4.2 - 77 K range [20] and attributed to recombination involving a higher energy radiative exciton state above the conduction band edge. Furthermore a blueshift in the reflection spectra near the band edge was observed from 4.2 to 200 K indicating a widening of the bandgap as temperature increases, with transitions possibly tracking with the band edge [20]. Therefore, the blueshift with increasing T for $CsPbCl_3$ below 100 K is attributed to the temperature-dependent bandgap widening. Above 100 K, however, the peak energies become invariant with temperature or redshift, although all peaks remain above the conduction band edge (Fig. 3b).

To determine the phonon energy, E_{ph}, the line broadening of the band edge PL emission for both compounds was measured as a function of temperature. The temperature dependence of peak width for excitonic peaks was analyzed using Toyozawa's equation [43,44]

$$\omega(T) = \frac{A}{\left[\exp\left(\frac{E_{ph}}{k_B T}\right) - 1\right]} + C \quad (3)$$

where $\omega(T)$ is the peak full-width half maximum (FWHM) and C is a constant linewidth at low temperatures due to the absence of phonon broadening. From the analysis of spectral data shown in Fig. 4a using Eqn. (3), a phonon energy E_{ph} of 0.016 eV was calculated for $CsPbBr_3$. This value is in good agreement with the value of a single phonon energy of 0.016 eV [15] as well as 0.019 eV [3], previously obtained for this material using Raman spectroscopy, .

Fig. 4b shows the plot of ω(T) vs T for $CsPbCl_3$. The curve, however, is discontinuous at lower temperature and likely due to a reported phase transition at ~185 K [45]. The material is tetragonal based on our single-crystal refinement at room temperature and possibly over the whole 194- 310 K range due to distortion of the perovskite structure. As a result of this structural phase change the data has only been fitted for the values from 185 K to 295 K. A value of 0.043 eV is calculated for E_{ph} using Eqn. (3). This value is in good agreement with a previously reported value of 0.046 eV for an LO phonon in $CsPbCl_3$ [46].

Thermal quenching of the PL intensity *I(T)* can be analyzed using the two-step quenching model [47]

$$I(T) = \frac{I_0}{1 + C_1 \exp\left(-\frac{E_1}{k_B T}\right) + C_2 \exp\left(-\frac{E_2}{k_B T}\right)} \qquad (4)$$

where I_0 is the peak intensity at 0 K, E_1 and E_2 are the high and low-temperature activation energies of non-radiative pathways, and C_1 and C_2 are related to the strength of the quenching processes. In the case of $CsPbBr_3$ the best fit analysis of the data in Fig. 5a to Eqn. (4) yields values of 0.017 eV and 0.0007 eV for E_1 and E_2, respectively. E_1 is often equated to the exciton binding energy [43,48] but in this case is about half as much as that previously reported for this compound [3,19]. Furthermore the agreement between the values obtained from Eq. 3 and Eq. 4 indicates that E_1 is the phonon energy.

For $CsPbCl_3$, values of 0.057 eV and 0.0076 eV for E_1 and E_2, respectively, were obtained from the least squares analysis of the data in Fig. 5b to Eqn. (4). The value of E_1 is in excellent agreement with the value of 0.052 eV reported by Belikovich et al for the activation energy of radiationless transitions in $CsPbCl_3$[21]. $CsPbX_3$ compounds have previously been reported to have large exciton binding energies, consistent with excitonic emissions persisting up to room temperature [3]. Their exciton binding energies are also consistent with those of semiconductors with similar bandgaps [49].

Power dependent PL Studies

The nature of recombination process can be determined from the dependence of the PL intensity on the excitation power [19]. It has been shown that the luminescence intensity I of the near-band-edge photoluminescence (NBEPL) emission lines is proportional to L^{γ}, where L is the power of the exciting laser radiation and the exponent γ is $1 < \gamma < 2$ for exciton-like transition and $\gamma < 1$ for free-to-bound and donor-acceptor pair (DAP) transitions[24]. All but one peak in the measured spectra have values of γ greater than 1 at low power (Figs. 6, 7). This indicates that the recombination involves excitons. The exception is the 2.98 eV peak in $CsPbCl_3$ with a γ-value of unity within error (γ = 0.94±0.15). The peak position, however, shows a blueshift as the excitation power is increased (Fig. 8b), which is not consistent with the behavior of a free to bound transition [50]. Thus it is concluded that the power dependent PL measurements for $CsPbX_3$ indicate that all peaks are excitonic in nature.

The plot of integrated PL intensity vs laser power for $CsPbBr_3$ in Fig. 6 indicates that while the signals increase in intensity in the 0-10 mW range, a clear reduction in emission intensity is evident when the sample is irradiated with an intensity higher than 10 mW. This is unexpected since PL intensity should increase with increasing laser intensity. There are two possible mechanisms which can produce this effect. Due to our experimental conditions of high excitation power, this behavior could be attributed to carrier scattering effects. For a high concentration of photo-excited carriers, screening, scattering or self-annihilation of excitons occurs, decreasing the overall PL intensity at high excitation [51]. The other possibility is that PL fatigue is present in the material, characterized by a reduction in PL signal intensity as a function of time under prolonged light irradiation [49]. Since the scans for each laser intensity level are done with only a few minutes between scans, it is possible that the material does not have time to equilibrate before being excited again. This PL fatigue has also previously been observed in other semiconductors including chalcogenide glasses [52], GaAs [53], and amorphous Si [54]. It should be noted, however, that PL fatigue has not been observed in $CsPbBr_3$ crystals and is currently under investigation to be presented elsewhere. The PL intensity reduction phenomenon was not observed in $CsPbCl_3$ in this study, possibly due to the lower excitation power that was used.

DFT Calculations

Calculations of the defect formation energy in $CsPbBr_3$ using density functional theory (DFT) indicate a series of defect levels attributed to native defects. In this study, we considered vacancies (V_{Cs}, V_{Pb}, V_{Br}) and antisite defects (Cs_{Pb}, Pb_{Cs}, Pb_{Br}, Br_{Pb}, Cs_{Br}, and Br_{Cs}). In Fig. 9(a),

ΔH_D of V_{Cs}, V_{Pb}, V_{Br}, Cs_{Pb}, Pb_{Cs}, Br_{Cs}, and Br_{Pb} are presented as a function of the Fermi energy E_F for three different growth conditions (Cs-poor only, Br-poor only, and a combination of Cs and Br deficiencies). The formation energies (ΔH_D) of the antisite defects Pb_{Br} and Cs_{Br} are high and they are unlikely to be present. Calculations indicate that V_{Cs}, V_{Pb} ,Cs_{Pb} ,and Br_{Cs}have shallow acceptor levels (≤ 0.1 eV) and V_{Br} and Pb_{Cs} donor levels with relatively low defect formation energy, in agreement with recent DFT defect studies on $CsPbBr_3$ and other halide perovskites [35,55]. In contrast, Br_{Pb} has deep acceptor levels at 1.40 eV and 1.61 eV within the gap; however its ΔH_D is high which again leads to a low concentration of this defect. Its maximum concentration under Cs-poor condition is 10^{13} cm^{-3} at 650K.

The most dominant defects are then V_{Cs}, V_{Pb}, Pb_{Cs} and V_{Br}. Of these, V_{Cs}, V_{Pb}, result in shallow levels within the bandgap, while V_{Br} and Pb_{Cs} have states ~0.23 eV and ~0.24 eV above the bandgap. These values for V_{Br} are in reasonable agreement with those recently reported by Shi and Du (0.16 eV, [35]) and supports the experimental PL peak positions in the current study. Fig. 9(b) summarizes calculated native defect levels of $CsPbBr_3$. It is worth noting here that our DFT calculations are still based on the GGA functional method and thus an accurate prediction of the enthalpies of formation (ΔH_f) is difficult. These calculations give indications concerning the nature of the defects but do not allow their unequivocal identification. Nevertheless, the fact that no significant concentration of stable charged defects are observed in $CsPbBr_3$ indicates potentially excellent charge transport properties in the form of high μτ values for efficient charge collection in detector devices.

IV. Conclusion

Above gap luminescence in single crystal perovskite compounds $CsPbX_3$ (X = Cl, Br) are observed. Power and temperature dependent photoluminescent properties are presented from 10 K up to 290 K. The power dependent PL studies indicate that all peaks are excitonic involving bound excitons for both compounds. Both compounds exhibit above-bandgap luminescence which blueshifts with increasing temperature. $CsPbBr_3$ luminescence shows evidence of a resonant state located 0.16 eV above the conduction band minimum, corresponding to the peak energy seen in the PL. This energy level is attributed to a Br vacancy on the basis of DFT calculations, which give indications concerning the nature of the defects. In both $CsPbBr_3$ and $CsPbCl_3$ all emission peaks undergo a blueshift with increasing temperature. For $CsPbBr_3$, phonon-assisted processes are responsible for the blueshift, while in $CsPbCl_3$ the blueshift is attributed to a widening of the bandgap. No significant deep level or DAP luminescent peaks are observed in the PL spectrum of the $CsPbX_3$ perovskite compounds. The results indicate that these Bridgman grown materials may be suitable for hard radiation detector applications due to the absence of radiative deep level defects that can serve as trapping centers.

ACKNOWLEDGEMENT

This work is supported by the U.S. Department of Energy (NNSA) under Contract DE-AC02-06CH11357. The theory part was supported by the Department of Homeland Security with grant 2010-DN-077-ARI042-02. The authors thank Kyle McCall for technical assistance.

List of Figure Captions

Fig. 1: (a) PL spectra of $CsPbBr_3$ from 10 K to 180 K. (inset) Two peaks are observed at 10 K, at 2.29 and 2.33 eV. A photograph of the green PL emission is also shown in the inset. (b) Spectra of $CsPbCl_3$ from 11 K to 290 K. (inset) at 11K (shown) and up to 100 K, 4 peaks are seen: 2.94, 2.96, 2.97, and 2.98 eV. Above 100 K, and up to 290 K all peaks except that at 2.94 eV are seen. A photograph of the blue PL emission is also shown in the inset. (c) Semi-log plots of the PL spectra of $CsPbBr_3$ and $CsPbCl_3$ over a wide sub-band-gap energy range and increased sensitivity.

Fig. 2: Plots of α^2 vs energy of (a) $CsPbBr_3$ and (b) $CsPbCl_3$ single crystals, calculated from transmission measurements at room temperature. (c) Powder absorption spectra of $CsPbX_3$ samples.

Fig. 3: (a) Peak position vs temperature, $CsPbBr_3$. The excitation intensity is 31.6 mW. The peak positions for both peaks are observed to blue-shift with increasing temperature. (b) Peak position vs. T, $CsPbCl_3$. The excitation intensity is 15.8 mW. The peak position is expected to continuously red-shift as T increases, but this is only observed above ~150 K, and is not seen for the peak at 2.98 eV. This blue shift seen in both compounds may result from carrier screening due to a large concentration of carriers generated by the high excitation intensity and thermal generation.

Fig. 4: (a) Peak FWHM vs T for $CsPbBr_3$. Fitting the data with Eqn. (1) yields values of 0.016 eV $E_{ph.}$ (b) Peak FWHM vs T, $CsPbCl_3$. Only the region from 190-300K can be fitted with Eqn. (1) since the material undergoes a phase transition at 185 K. The analysis yields values of 0.043 eV for $E_{ph.}$

Fig. 5: (a) Peak intensity vs 1/T, $CsPbBr_3$. Analysis of this data with Eqn. (2) indicates that the high and low temperature activation energies are is 0.017 and 0.0007 eV. (b) Peak intensity vs 1/T, $CsPbCl_3$. Analysis of this data indicates that the high and low temperature activation energies are is 0.057 and 0.0076 eV.

Fig. 6: A plot of log (PL intensity) vs log (incident laser intensity), $CsPbBr_3$. A linear fit of the low excitation region (solid line) shows slopes of 1.5 and 1.4 for peaks centered at 2.29 eV and 2.33 eV, respectively. The PL intensity decreases, however, above an incident laser power of 10 mW for the shoulder peak, and 31.6 mW for the main peak.

Fig. 7: log PL intensity vs log laser power for the 3 peaks seen at higher temperatures in $CsPbCl_3$. The laser intensity was varied from 2 to 50 mW. Linear fits are shown by the solid black lines. The γ values are 1.75 for (a), 1.57 for (b), and 0.94 for (c). These correspond to the peaks at 2.96, 2.97, and 2.98 eV respectively.

Fig. 8: (a) Peak position vs. incident laser power for $CsPbBr_3$ at 10 K. (b) Peak position vs. laser power, $CsPbCl_3$ at 10K.

Fig. 9: (a) Calculated defect formation energy in the $CsPbBr_3$ are plotted as a function of Fermi level. Left and right panels correspond to Cs-poor and Br-poor conditions, respectively. The middle panel is plotted for the mid-condition between Cs-poor and Br-poor. Equilibrium Fermi level E_F^{eq} is plotted as black vertical dotted-line. (b) Defect levels for vacancy and antisite defect of $CsPbBr_3$ are summarized. Defect levels are presented with respect to the valence band maximum. Blue and red at the bottom of figure means acceptor and donor type, respectively.

Figures

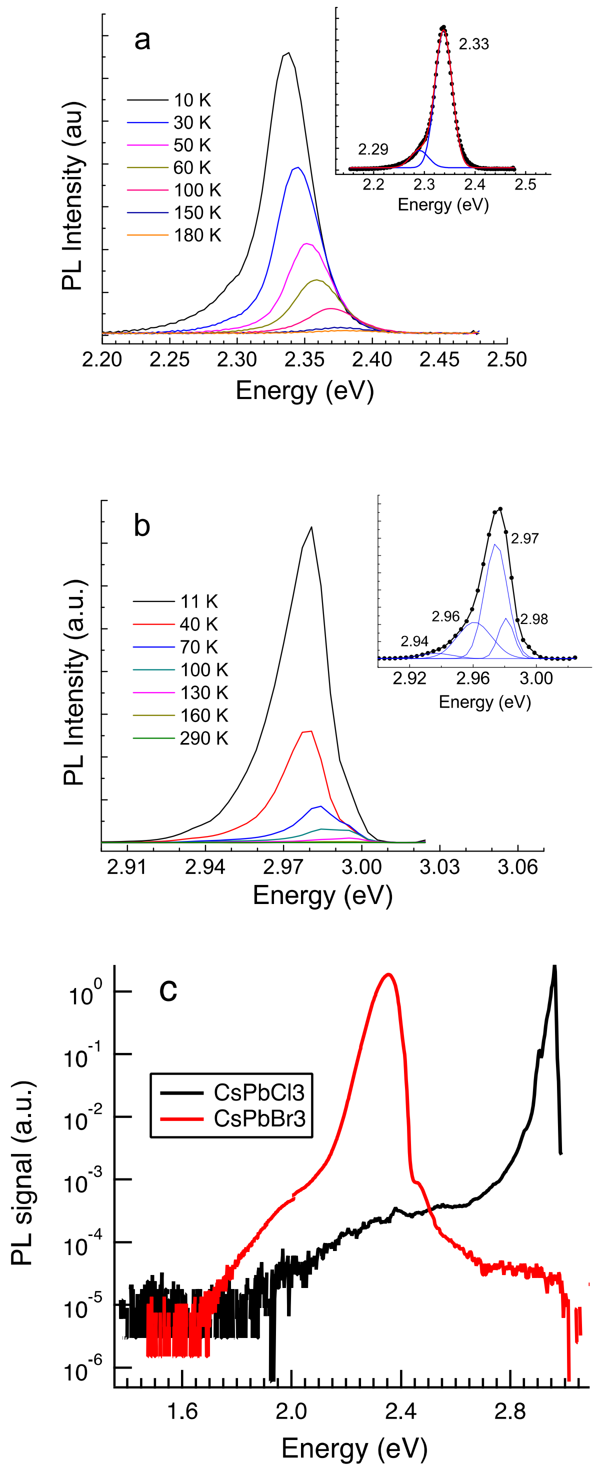

Figure 1

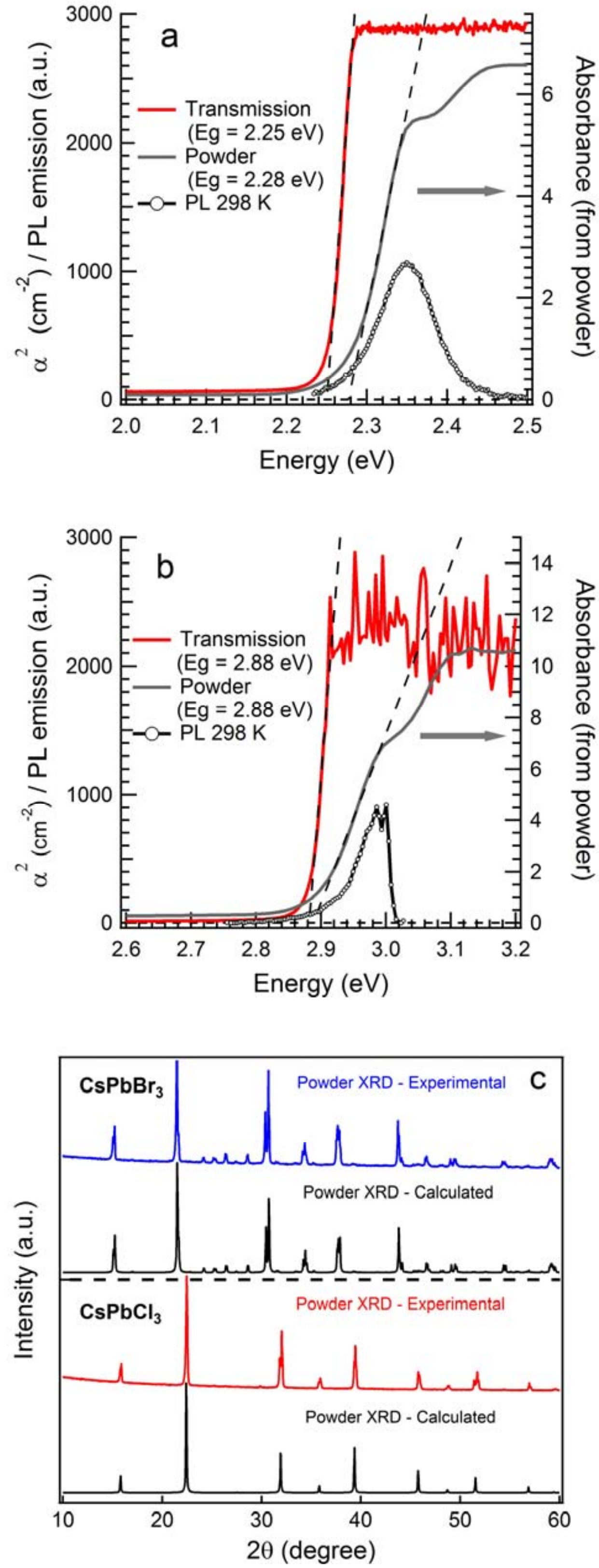
a
Transmission
(Eg = 2.25 eV)
Powder
(Eg = 2.28 eV)
PL 298 K
α^2 (cm^{-2}) / PL emission (a.u.)
Absorbance (from powder)
Energy (eV)
b
Transmission
(Eg = 2.88 eV)
Powder
(Eg = 2.88 eV)
PL 298 K
α^2 (cm^{-2}) / PL emission (a.u.)
Absorbance (from powder)
Energy (eV)
C
$CsPbBr_3$
Powder XRD - Experimental
Powder XRD - Calculated
$CsPbCl_3$
Powder XRD - Experimental
Powder XRD - Calculated
Intensity (a.u.)
2θ (degree)

Figure 2

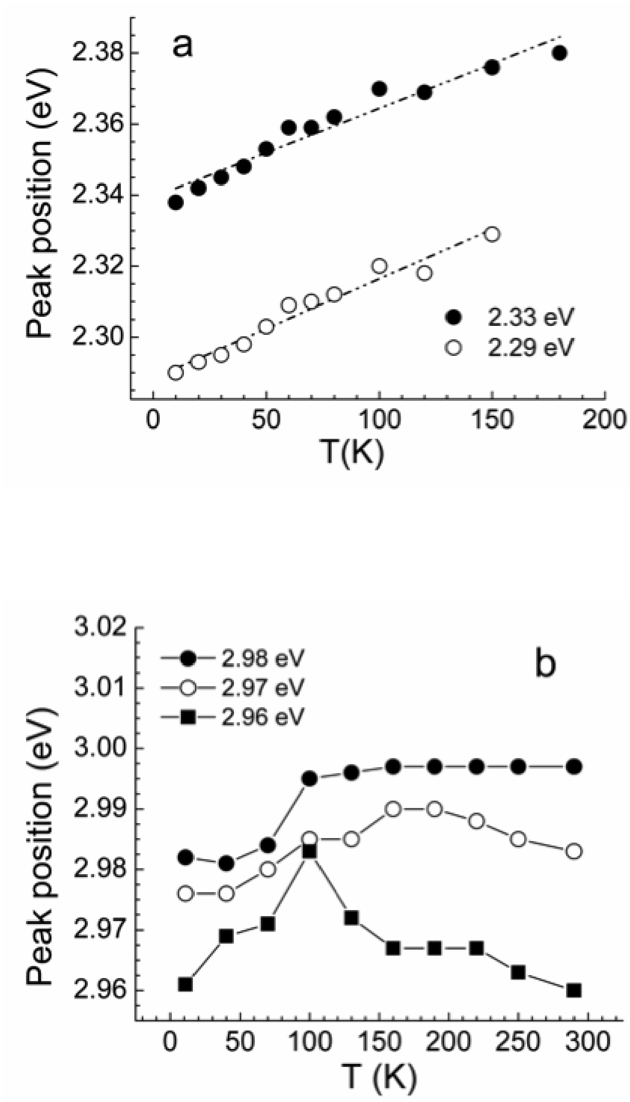
a
Peak position (eV)
2.38
2.36
2.34
2.32
2.30
2.33 eV
2.29 eV
0
50
100
150
200
T(K)
b
Peak position (eV)
3.02
3.01
3.00
2.99
2.98
2.97
2.96
2.98 eV
2.97 eV
2.96 eV
0
50
100
150
200
250
300
T (K)

Figure 3

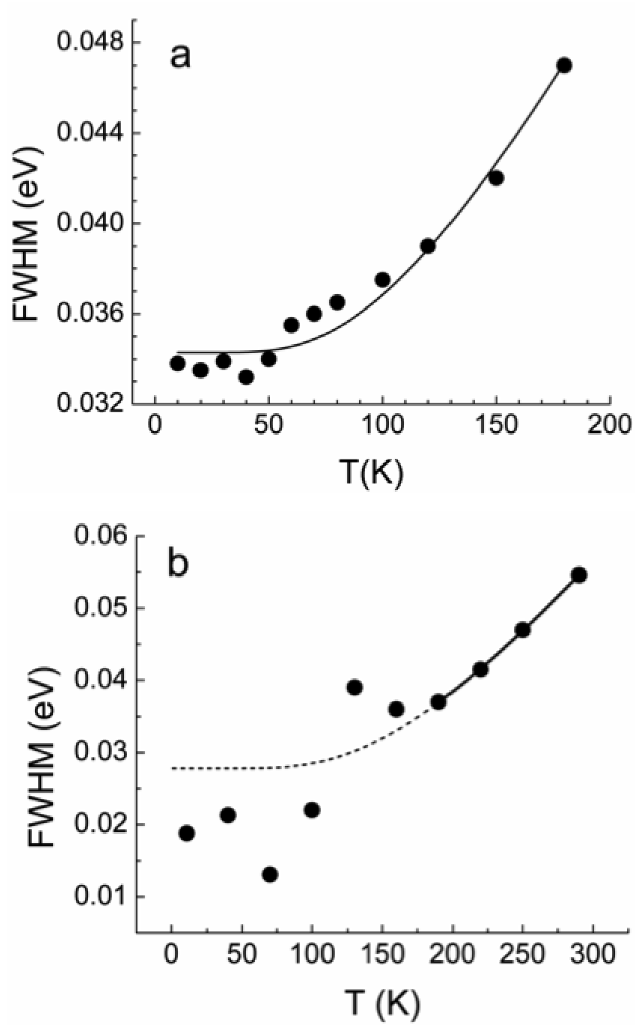
a
FWHM (eV)
0.048
0.044
0.040
0.036
0.032
0
50
100
150
200
T(K)
b
FWHM (eV)
0.06
0.05
0.04
0.03
0.02
0.01
0
50
100
150
200
250
300
T (K)

Figure 4

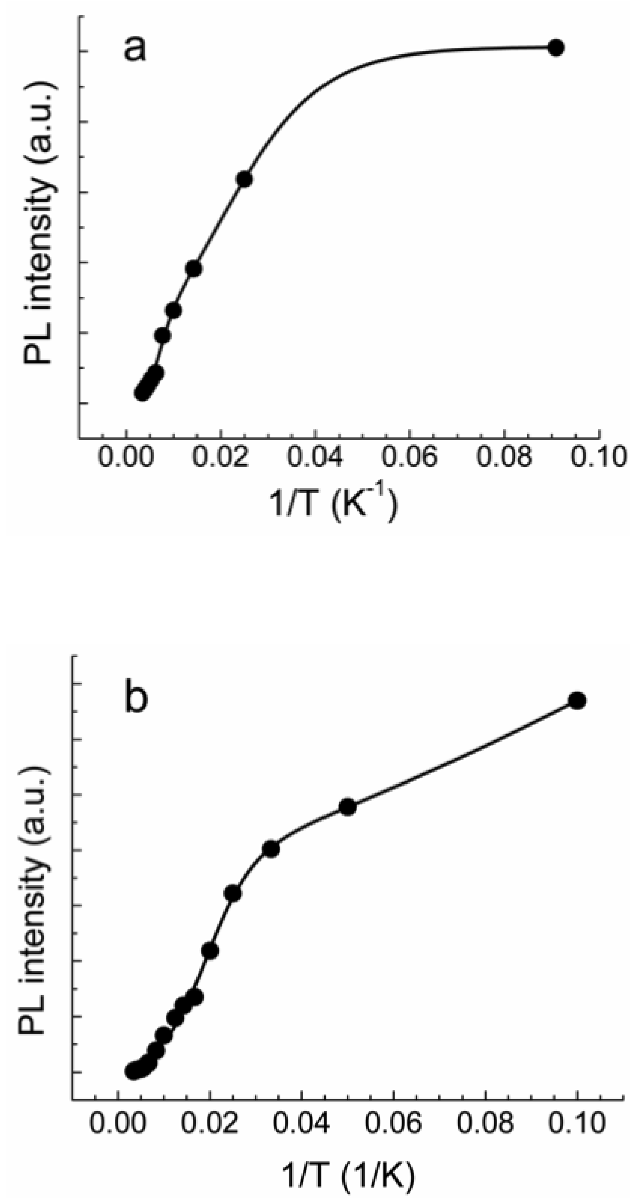
a
PL intensity (a.u.)
0.00
0.02
0.04
0.06
0.08
0.10
1/T (K-1)
b
PL intensity (a.u.)
0.00
0.02
0.04
0.06
0.08
0.10
1/T (1/K)

Figure 5

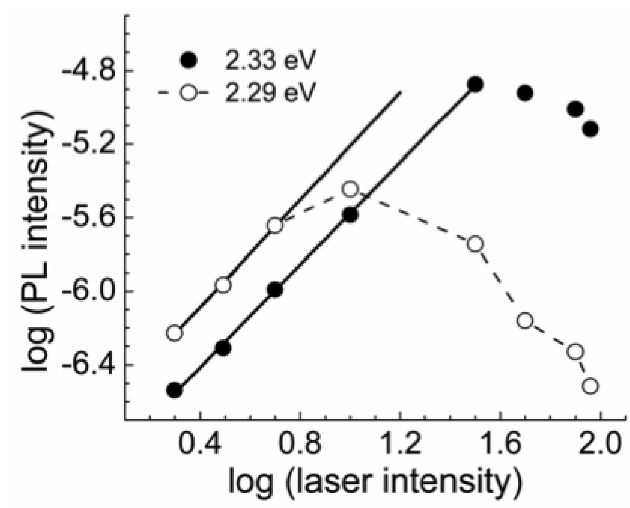
2.33 eV
2.29 eV
log (PL intensity)
-4.8
-5.2
-5.6
-6.0
-6.4
0.4
0.8
1.2
1.6
2.0
log (laser intensity)

Figure 6.

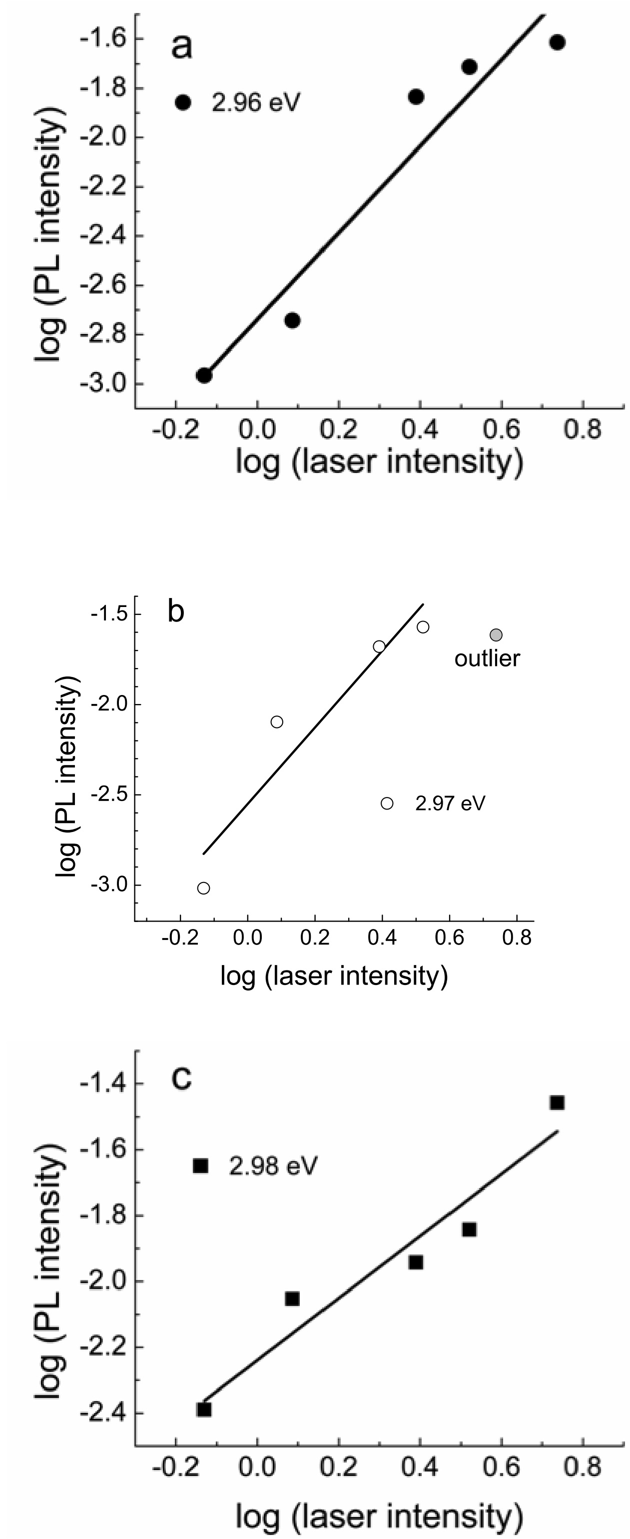
a
2.96 eV
log (PL intensity)
log (laser intensity)
-1.6
-1.8
-2.0
-2.2
-2.4
-2.6
-2.8
-3.0
-0.2
0.0
0.2
0.4
0.6
0.8
b
outlier
2.97 eV
log (PL intensity)
log (laser intensity)
-1.5
-2.0
-2.5
-3.0
-0.2
0.0
0.2
0.4
0.6
0.8
c
2.98 eV
log (PL intensity)
log (laser intensity)
-1.4
-1.6
-1.8
-2.0
-2.2
-2.4
-0.2
0.0
0.2
0.4
0.6
0.8

Figure 7.

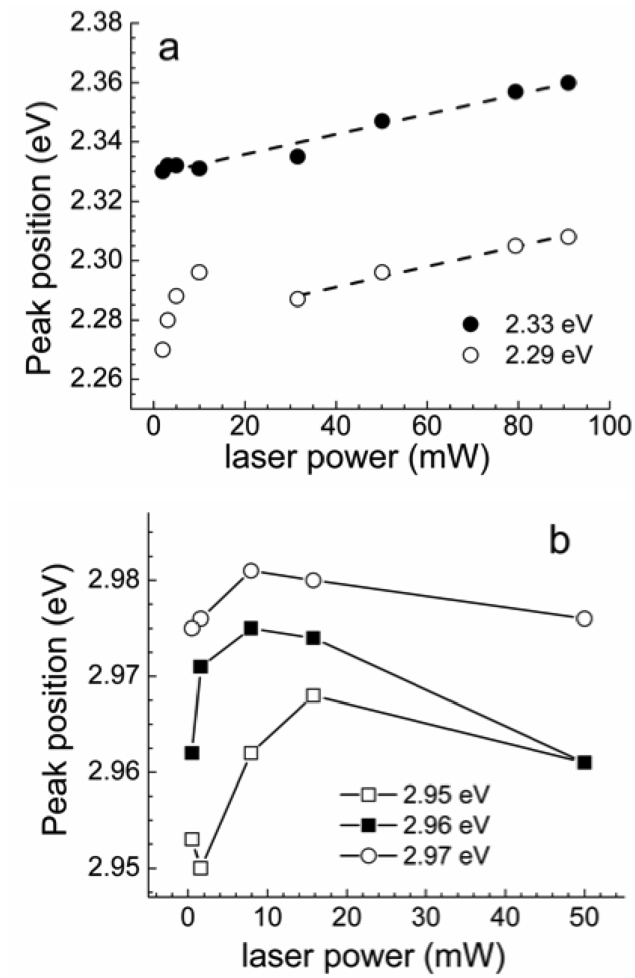
a
Peak position (eV)
2.38
2.36
2.34
2.32
2.30
2.28
2.26
0
20
40
60
80
100
laser power (mW)
2.33 eV
2.29 eV
b
Peak position (eV)
2.98
2.97
2.96
2.95
0
10
20
30
40
50
laser power (mW)
2.95 eV
2.96 eV
2.97 eV

Figure 8.

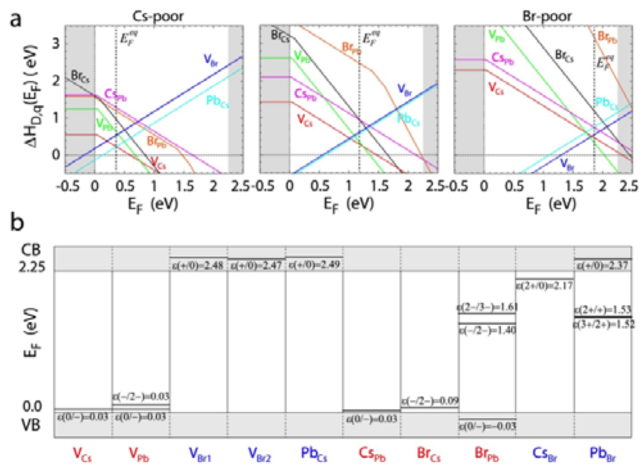
a
Cs-poor
Br-poor
E_F^{eq}
$\Delta H_{D,q}(E_F)$ (eV)
E_F (eV)
b
CB
2.25
0.0
VB
E_F (eV)
ε(+/0)=2.48
ε(+/0)=2.47
ε(+/0)=2.49
ε(2−/3−)=1.61
ε(−/2−)=1.40
ε(2+/0)=2.17
ε(+/0)=2.37
ε(2+/+)=1.53
ε(3+/2+)=1.52
ε(−/2−)=0.03
ε(0/−)=0.03
ε(0/−)=0.03
ε(0/−)=0.03
ε(−/2−)=0.09
ε(0/−)=−0.03
V_{Cs}
V_{Pb}
V_{Br1}
V_{Br2}
Pb_{Cs}
Cs_{Pb}
Br_{Cs}
Br_{Pb}
Cs_{Br}
Pb_{Br}

Figure 9.

References

1 C. K. Moller, *Nature* **182** (4647), 1436 (1958).

2 C. K. Moller, *Mat. Fys. Medd. Dan. Vid. Selsk* **32** (2), 1-27 (1959); C. K. Moller, *Mat. Fys. Medd. Dan. Vid. Selsk* **32** (1), 1-18 (1959).

3 I. P. Pashuk, N. S. Pidzyrailo, and M. G. Matsko, *Sov. Phys. Solid State* **23** (7), 1263 (1981).

4 S. J. Clark, J. D. Donaldson, and J. A. Harvey, *Journal of Materials Chemistry* **5** (11), 1813-1818 (1995); F. Somma, M. Nikl, K. Nitsch, P. Fabeni, and G. P. Pazzi, *Journal of Luminescence* **94–95** (0), 169-172 (2001); T. Sakuma, M. Mutou, K. Ohki, M. Arai, H. Takahashi, and Y. Ishii, *Solid State Ionics* **154–155**, 237-242 (2002); S.-i. Kondo, M. Kakuchi, A. Masaki, and T. Saito, *Journal of the Physical Society of Japan* **72** (7), 1789-1791 (2003); S. Kondo, K. Suzuki, T. Saito, H. Asada, and H. Nakagawa, *Physical Review B* **70** (20), 205322 (2004); S. Kondo, K. Takahashi, T. Nakanish, T. Saito, H. Asada, and H. Nakagawa, *Current Applied Physics* **7** (1), 1-5 (2007).

5 K. Nitsch, V. Hamplová, M. Nikl, K. Polák, and M. Rodová, *Chemical Physics Letters* **258** (3–4), 518-522 (1996).

6 M. Nikl, K. Nitsch, E. Mihóková, K. Polák, P. Fabeni, G. P. Pazzi, M. Gurioli, S. Santucci, R. Phani, A. Scacco, and F. Somma, *Physica E: Low-dimensional Systems and Nanostructures* **4** (4), 323-331 (1999).

7 Y. H. Chang, C. H. Park, and K. Matsuishi, *Journal of the Korean Physical Society* **44** (4), 889-893 (2004); G. Murtaza and I. Ahmad, *Physica B: Condensed Matter* **406** (17), 3222-3229 (2011).

8 M. Natarajan and B. Prakash, *physica status solidi (a)* **4** (3), K167-K172 (1971); M. I. Cohen, K. F. Young, T. T. Chang, and W. S. Brower, *Journal of Applied Physics* **42** (13), 5267-5272 (1971); S. Hirotsu, J. Harada, M. Iizumi, and K. Gesi, *Journal of the Physical Society of Japan* **37** (5), 1393-1398 (1974); J. Hutton, R. J. Nelmes, G. M. Meyer, and V. R. Eiriksson, *Journal of Physics C: Solid State Physics* **12** (24), 5393 (1979); M. Sakata, T. Nishiwaki, and J. Harada, *Journal of the Physical Society of Japan* **47** (1), 232-233 (1979); M. Sakata, J. Harada, M. J. Cooper, and K. D. Rouse, *Acta Crystallographica Section A* **36** (1), 7-15 (1980).

9 A. Kojima, K. Teshima, Y. Shirai, and T. Miyasaka, *Journal of the American Chemical Society* **131** (17), 6050-6051 (2009).

10 I. Chung, B. Lee, J. He, R. P. H. Chang, and M. G. Kanatzidis, *Nature* **485** (7399), 486-489 (2012).

11 L. Etgar, P. Gao, Z. Xue, Q. Peng, A. K. Chandiran, B. Liu, M. K. Nazeeruddin, and M. Grätzel, *Journal of the American Chemical Society* **134** (42), 17396-17399 (2012); H.-S. Kim, C.-R. Lee, J.-H. Im, K.-B. Lee, T. Moehl, A. Marchioro, S.-J. Moon, R. Humphry-Baker, J.-H. Yum, J. E. Moser, M. Gratzel, and N.-G. Park, *Sci. Rep.* **2**, 591 (2012); M. M. Lee, J. Teuscher, T. Miyasaka, T. N. Murakami, and H. J. Snaith, *Science* **338** (6107), 643-647 (2012).

12 H. Zhou, Q. Chen, G. Li, S. Luo, T.-b. Song, H.-S. Duan, Z. Hong, J. You, Y. Liu, and Y. Yang, *Science* **345** (6196), 542-546 (2014).

13 O. Busmundrud and J. Feder, *Solid State Communications* **9** (18), 1575-1577 (1971); J. Mizusaki, K. Arai, and K. Fueki, *Solid State Ionics* **11** (3), 203-211 (1983); R. L. Narayan, M. V. S. Sarma, and S. V. Suryanarayana, *Journal of Materials Science Letters* **6** (1), 93-94 (1987).

14 Z. Liu, J. A. Peters, C. C. Stoumpos, M. Sebastian, B. W. Wessels, J. Im, A. J. Freeman, and M. G. Kanatzidis, *Proc. SPIE* **8852**, 88520A (2013).

15 C. C. Stoumpos, C. D. Malliakas, J. A. Peters, Z. Liu, M. Sebastian, J. Im, T. C. Chasapis, A. C. Wibowo, D. Y. Chung, A. J. Freeman, B. W. Wessels, and M. G. Kanatzidis, *Cryst. Growth Des.* **13** (7), 2722-2727 (2013).

16 S. Wang, Z. Liu, J. A. Peters, M. Sebastian, S. L. Nguyen, C. D. Malliakas, C. C. Stoumpos, J. Im, A. J. Freeman, B. W. Wessels, and M. G. Kanatzidis, *Cryst. Growth Des.* **14** (5), 2401-2410 (2014).

17 A. Owens, *Compound Semiconductor Radiation Detectors*. (Taylor & Francis, 2012).

18 K. Hitomi, Y. Kikuchi, T. Shoji, and K. Ishii, *Nuclear Science, IEEE Transactions on* **56** (4), 1859-1862 (2009).

19 D. Fröhlich, K. Heidrich, H. Künzel, G. Trendel, and J. Treusch, *Journal of Luminescence* **18–19, Part 1**, 385-388 (1979).

20 L. N. Amitin, A. T. Anistratov, and A. I. Kuznetsov, *Fiz. Tverd. Tela (Leningrad)* **21** (12), 3535-3541 (1979).

21 B. A. Belikovich, I. P. Pashchuk, and N. S. Pidzyrailo, *Optics and Spectroscopy* **42**, 62-64 (1977).

22 K. Goksen, N. M. Gasanly, and R. Turan, *Crystal Research and Technology* **41** (8), 822-828 (2006).

23 J. Krustok, H. Collan, and K. Hjelt, *Journal of Applied Physics* **81** (3), 1442-1445 (1997).

24 T. Schmidt, K. Lischka, and W. Zulehner, *Physical Review B* **45** (16), 8989-8994 (1992); A. Bauknecht, S. Siebentritt, J. Albert, and M. C. Lux-Steiner, *Journal of Applied Physics* **89** (8), 4391-4400 (2001).

25 G. M. Sheldrick, *Acta Crystallographica Section A* **64** (1), 112-122 (2008).

26 A. L. Spek, *Acta Crystallographica Section D* **65** (2), 148-155 (2009).

27 L. Farrugia, *Journal of Applied Crystallography* **45** (4), 849-854 (2012).

28 P. E. Blöchl, *Physical Review B* **50** (24), 17953-17979 (1994).

29 G. Kresse and J. Hafner, *Physical Review B* **47** (1), 558-561 (1993); G. Kresse and J. Furthmüller, *Physical Review B* **54** (16), 11169-11186 (1996).

30 J. P. Perdew, K. Burke, and M. Ernzerhof, *Physical Review Letters* **77** (18), 3865-3868 (1996).

31 J. Heyd, G. E. Scuseria, and M. Ernzerhof, *The Journal of Chemical Physics* **118** (18), 8207-

8215 (2003); J. Heyd, G. E. Scuseria, and M. Ernzerhof, *The Journal of Chemical Physics* **124** (21), 219906 (2006).

32 C. Freysoldt, B. Grabowski, T. Hickel, J. Neugebauer, G. Kresse, A. Janotti, and C. G. Van de Walle, *Reviews of Modern Physics* **86** (1), 253-305 (2014).

33 S. Lany and A. Zunger, *Physical Review B* **78** (23), 235104 (2008).

34 D. Åberg, P. Erhart, A. J. Williamson, and V. Lordi, *Physical Review B* **77** (16), 165206 (2008).

35 H. Shi and M.-H. Du, *Physical Review B* **90** (17), 174103 (2014).

36 Q. Dong, Y. Fang, Y. Shao, P. Mulligan, J. Qiu, L. Cao, and J. Huang, *Science* **347** (6225), 967-970 (2015).

37 P. H. Tan, X. D. Luo, Z. Y. Xu, Y. Zhang, A. Mascarenhas, H. P. Xin, C. W. Tu, and W. K. Ge, *Phys. Rev. B* **73** (20), 205205 (2006).

38 D. R. Scifres, N. Holonyak, C. B. Duke, G. G. Kleiman, A. B. Kunz, M. G. Craford, W. O. Groves, and A. H. Herzog, *Phys. Rev. Lett.* **27** (4), 191-194 (1971).

39 A. Voloshinovskii, S. Myagkota, A. Gloskovskii, and S. Zazubovich, *physica status solidi (b)* **225** (1), 257-264 (2001).

40 P. Lautenschlager, P. B. Allen, and M. Cardona, *Physical Review B* **31** (4), 2163-2171 (1985).

41 V. D'Innocenzo, G. Grancini, M. J. P. Alcocer, A. R. S. Kandada, S. D. Stranks, M. M. Lee, G. Lanzani, H. J. Snaith, and A. Petrozza, *Nat Commun* **5** (2014); N. Ashcroft, *Saunders College, Philadelphia* (1976).

42 H. Younghun, U. Youngho, and P. Hyoyeol, *Journal of the Korean Physical Society* **58** (51), 1312 (2011).

43 C. J. Youn, T. S. Jeong, M. S. Han, and J. H. Kim, *Journal of Crystal Growth* **261** (4), 526-532 (2004).

44 Y. Toyozawa, *Progress of Theoretical Physics* **27** (1), 89-104 (1962).

45 K. Wu, A. Bera, C. Ma, Y. Du, Y. Yang, L. Li, and T. Wu, *Physical Chemistry Chemical Physics* **16** (41), 22476-22481 (2014).

46 D. M. Calistru, L. Mihut, S. Lefrant, and I. Baltog, *Journal of Applied Physics* **82** (11), 5391-5395 (1997).

47 D. Bimberg, M. Sondergeld, and E. Grobe, *Physical Review B* **4** (10), 3451-3455 (1971).

48 E. Cohen, R. A. Street, and A. Muranevich, *Physical Review B* **28** (12), 7115-7124 (1983).

49 I. Pelant and J. Valenta, *Luminescence Spectroscopy of Semiconductors*. (Oxford University Press, New York, 2012).

50 S. Levcenko, V. E. Tezlevan, E. Arushanov, S. Schorr, and T. Unold, *Physical Review B* **86** (4), 045206 (2012).

51 D. C. Reynolds, D. C. Look, and B. Jogai, *Journal of Applied Physics* **88** (10), 5760-5763 (2000); T.-R. Park, *Journal of the Korean Physical Society* **44** (4), 930-933 (2004).

52 T. Nakanishi, Y. Tomii, and K. Hachiya, *Electrochimica Acta* **100**, 304-310 (2013); T.

Nakanishi, Y. Tomii, and K. Hachiya, *Journal of Non-Crystalline Solids* **354** (15-16), 1627-1632 (2008); M. Seki and K. Hachiya, *Journal of Physics: Condensed Matter* **15** (26), 4555 (2003).

53 D. Redfield and R. H. Bube, *Photoinduced Defects in Semiconductors*. (Cambridge University Press, 1996).

54 I. Hirabayashi, K. Morigaki, and S. Nitta, *Japanese Journal of Applied Physics* **19** (7), L357 (1980); D. Redfield and R. H. Bube, *Applied Physics Letters* **54** (11), 1037-1039 (1989).

55 W.-J. Yin, T. Shi, and Y. Yan, *Applied Physics Letters* **104** (6), 063903 (2014).